

Cosmology in the non-linear regime : the small scale miracle

Fabien Lacasa^{*1}

Institut d'Astrophysique Spatiale (IAS), Bâtiment 121, F-91405 Orsay, Université Paris-Sud 11 and CNRS, UMR 8617, France

December 7, 2022

ABSTRACT

Interest rises to exploit the full shape information of the galaxy power spectrum, as well as pushing analyses to smaller non-linear scales. Here I use the halo model to quantify the information content in the tomographic angular power spectrum of galaxies $C_\ell^{\text{gal}}(i_z)$, for future high resolution surveys : *Euclid* and *SKA2*. I study how this information varies as a function of the scale cut applied, either with angular cut ℓ_{max} or physical cut k_{max} . For this, I use analytical covariances with the most complete census of non-Gaussian terms, which proves critical. I find that the Fisher information on most cosmological and astrophysical parameters follows a striking behaviour. Beyond the perturbative regime we first get decreasing returns : the information keeps rising but the slope slows down until reaching a saturation. The location of this plateau is a bit beyond the reach of current modeling methods : $k \sim 2 \text{ Mpc}^{-1}$ and slightly depends on the parameter and redshift bin considered. I explain the origin of this plateau, which is due to non-linear effects both on the power spectrum, and more importantly on non-Gaussian covariance terms. Then, pushing further on I find that information rises again in the highly non-linear regime. I find that the cosmological information in this small scale miracle can indeed be disentangled from astrophysical information and yield large improvements. Pushing *SKA2* analysis from $k_{\text{max}} = 1 \text{ Mpc}^{-1}$ to $k_{\text{max}} = 10 \text{ Mpc}^{-1}$ can improve the error bar on σ_8 by a factor 9 and the error bar on the Dark Energy equation of state w_0 by a factor 5. Finally I show that high order statistics beyond the power spectrum should yield further significant improvements in this regime, with the improvements increasing when pushing k_{max} . Data and notebooks reproducing all plots and results will be made available at <https://github.com/fabienlacasa/SmallScaleMiracle>

Key words. methods: analytical - large-scale structure of the universe

1. Introduction

Future surveys of the large scale structure such as *Euclid* (Lau-reijs et al. 2011), *LSST* (Abell et al. 2009) and *SKA* (Maartens et al. 2015) will allow high resolution mapping of the distribution of galaxies in the Universe. Exploiting the most out of these data sets would require to (i) use the full shape of the statistical measurements, in contrast for instance with targeted BAO extraction, and (ii) push the analyses to the smallest accessible scales.

Full shape information of the galaxy power spectrum can indeed extract information from faint features (e.g. Tansella 2018) but also from the general slope (to constrain n_s), and from the amplitude (to constrain σ_8 and the growth of structure) if used in conjunction with weak lensing or higher order correlation (Hoffmann et al. 2015). This has been shown to encode more constraining power than usual BAO and RSD analyses (Loureiro et al. 2019; Tröster et al. 2019).

Pushing to small scales is challenging for future surveys because they are entering the non-linear regime of structure formation where the physics of the dark matter halos become relevant. There is however a wealth of evidence that the halo properties do encode cosmological information to constrain Dark Energy and Gravity (Balmès et al. 2014; Lopes et al. 2018, 2019; Contigiani et al. 2019; Ryu & Lee 2019). This motivates rising interest to use non-linear scales for cosmological constraints (Lange et al. 2019, e.g.).

For the matter field, various methods have been developed to predict $P(k)$ to smaller scales with the required 1% precision, for

instance the *Euclid* emulator can reach $k \sim 5h/\text{Mpc}$ (Knabenhans et al. 2019) for ΛCDM , and fitting functions are proposed to push to $k \sim 10/\text{Mpc}$ (Hannestad & Wong 2019). This 1% target can also be reached for models beyond ΛCDM —including Dark Energy, Modified Gravity and neutrinos—through rescaling methods based on the halo model (Cataneo et al. 2019b; Giblin et al. 2019; Cataneo et al. 2019a).

For galaxy clustering, the situation is complexified by the galaxy formation physics. Halo model-based approaches are however showing their strength to extract cosmology out of galaxy statistics either with machine learning methods (Ntampaka et al. 2019), or with analytical Halo Occupation Distribution Kobayashi et al. (2019).

Targeting non-linear scales also brings the difficulty from a more complex statistic: the matter/galaxy density field becomes significantly non-Gaussian, which increases the error bars due to non-Gaussian covariance terms. In this article, I build up on Lacasa (2018, 2019) which allow a near complete modeling of these non-Gaussian terms using the halo model and Halo Occupation Distribution.

The question then rises of how much statistical power is indeed contained in these non-linear scales. And further, how much of this statistical power can effectively be harnessed for cosmological constraints. One could indeed intuitively think that most of this power would only constrain astrophysical/galaxy formation parameters. The purpose of this article is thus to investigate how much cosmological information, in particular on Dark Energy, is contained in the galaxy 2-point function depending on the range of scales of analysis, accounting both for the astrophysical dependence and the rising non-Gaussianity of the

^{*} fabien.lacasa@u-psud.fr

field. I will apply this specifically for the tomographic angular power spectrum, and for surveys with a high enough galaxy density that shot-noise is subdominant.

In describe the modeling and analytical equations in section 2, first stating the surveys I consider and the observational specification in Sect. 2.1, then the halo modeling of the galaxy distribution in Sect. 2.2, followed in Sect. 2.3 by a recapitulation of the equations of non-Gaussian covariance terms and first results on the behaviour of the power spectrum and its covariance terms when pushing in the highly non-linear regime. In section 3 I use Fisher forecasts to show the cosmological information content of the power spectrum as a function of scale, first in terms of multipoles in Sect. 3.1 and then translated into physical cuts k_{\max} in Sect. 3.2, before providing a physical interpretation of the results in Sect. 3.3. In section 4 I give an estimate of the information contained beyond the power spectrum and how it depends on scale. Finally I discuss the results and their potential consequences in section 5.

Throughout the article I adopt as fiducial cosmology flat Λ CDM with *Planck* 2018 cosmological parameters (Planck Collaboration et al. 2018) : $(\Omega_b h^2, \Omega_c h^2, H_0, n_s, \sigma_8, w_0) = (0.022, 0.12, 67, 0.96, 0.81, -1)$.

I will make available at <https://github.com/fabienlacasa/SmallScaleMiracle> the data and Python notebooks that allow to reproduce all plots and results of the article, and some more.

2. Halo modeling C_ℓ^{gal} and its covariance

2.1. Survey specifications and setup

I consider two mock galaxy surveys for the forecasts: the *Euclid* photometric sample and the *SKA2* galaxy survey where galaxies are detected as point sources in the HI intensity map.

For the *SKA2* sample I use specifications from (Bull 2016): a sky coverage of $15'000 \text{ deg}^2$ and a galaxy number density given by Table 3 of Bull (2016) that I interpolated at all necessary redshifts. The total density is $\sim 9 \text{ gals/arcmin}^2$ in the redshift range $[0, 2]$. I divide the sample into 10 equi-populated redshift bins, finding that the corresponding bin stakes are $z = 0.1, 0.198, 0.267, 0.33, 0.393, 0.461, 0.537, 0.628, 0.748, 0.934, 2$.

For the *Euclid* sample, I use specifications from (Laureijs et al. 2011; Euclid Collaboration et al. 2019): a sky coverage $f_{\text{SKY}} = 0.36$, a galaxy number density

$$n(z) \propto \left(\frac{z}{z_0}\right)^2 \exp\left[-\left(\frac{z}{z_0}\right)^{3/2}\right] \quad (1)$$

where $z_0 = z_m/\sqrt{2}$ with $z_m = 0.9$ the median redshift (Laureijs et al. 2011). The total density is 30 gals/arcmin^2 in the redshift range $[0, 2.5]$. Following Euclid Collaboration et al. (2019), I divide the sample into 10 equi-populated redshift bins, whose bin stakes are $z = 0.001, 0.418, 0.56, 0.678, 0.789, 0.9, 1.019, 1.155, 1.324, 1.576, 2.5$.

In the article I will show only plots for the *SKA2* case, as the plots for the *Euclid* sample are all qualitatively similar, and the scientific conclusions are the same. I will make available online the plots for both surveys on <https://github.com/fabienlacasa/SmallScaleMiracle>.

For both surveys, the forecasts are produced with a binning of multipoles, as is customary in data analysis. Specifically, I define 50 bins spaced logarithmically in the range $[30, 50000]$.

The binning operator is then defined by

$$P_{b,\ell} = \begin{cases} \frac{w_\ell}{w_{\ell_{\text{cen}}} \Delta\ell} & \text{if } \ell \in \text{bin}(b) \\ 0 & \text{otherwise} \end{cases} \quad (2)$$

with ℓ_{cen} the center of the multipole bin and w_ℓ a weighting scheme. Here I adopt the simple scheme $w_\ell = \ell$ which makes $w_\ell C_\ell$ roughly constant and thus improves the binning approximation.

The binned power spectrum and covariance are then given by

$$C_b = P_{b,\ell} C_\ell \quad (3)$$

$$\text{Cov}(C_b, C_{b'}) = P_{b,\ell} P_{b',\ell'} C_{\ell,\ell'} \quad (4)$$

I use these equations to bin the power spectrum and the Gaussian part of the covariance, which is diagonal. I have however found these equations to be too numerically intensive to be used for the non-Gaussian parts of the covariance when reaching tens of thousands of multipoles. Indeed, for 10 redshift bins, that would require computing $\mathcal{O}(10^{10-11})$ covariance elements before binning them. Instead, for these terms I have used the approximation that the correlation matrix varies smoothly within the bin so that the binned correlation can be approximated by the correlation at the central multipole ℓ_{cen} . I have checked that this approximation works to percent precision on parameter forecasts up to $\ell_{\max} = 2000$, which is the limit where I could push the brute force computation. In the following, for simplicity binned quantities will be plotted at the center of the multipole bin.

2.2. Halo modeling

I use the standard halo model, as reviewed for instance by Cooray & Sheth (2002). In terms of ingredients, I use the halo mass function from Tinker et al. (2008) with the corresponding halo bias from Tinker et al. (2010). I model the distribution of galaxies using the Halo Occupation Distribution (HOD). Specifically I adopt one similar to Zehavi et al. (2011) : $N_{\text{gal}} = N_{\text{cen}} + N_{\text{sat}}$, where the central galaxy follows a Bernoulli distribution with probability

$$P(N_{\text{cen}} = 1) = \frac{1}{2} \left(1 + \text{Erf} \left(\frac{\log_{10} M - \log_{10} M_{\min}}{\sigma_{\log M}} \right) \right) \quad (5)$$

and the satellite galaxies follow a Poisson distribution for the satellite galaxies, conditioned to the presence of the central, with mean

$$\mathbb{E}[N_{\text{sat}} | N_{\text{cen}} = 1] = \left(\frac{M}{M_{\text{sat}}} \right)^{\alpha_{\text{sat}}} \quad (6)$$

The specifications for the galaxy redshift distribution $n(z)$ given in Sect. 2.1 do not correspond to a volume-limited sample, i.e. constant HOD parameters. To deal with this, I follow the approach of Lacasa (2019) by fitting the HOD at each redshift. Specifically, I fit the M_{\min} parameter, assuming that the ratio $M_{\text{ratio}} = M_{\text{sat}}/M_{\min} = 10$ is constant and that $\sigma_{\log M} = 0.5$ and $\alpha_{\text{sat}} = 1$ are constant. The resulting function $M_{\min}(z)$ is then further fitted with a fourth order polynomial:

$$M_{\min}(z) = M_{\min}^a + M_{\min}^b z + M_{\min}^c z^2 + M_{\min}^d z^3. \quad (7)$$

Lacasa (2019) showed that this redshift-dependent gives a $\sim 2.5\%$ fit to $n(z)$ on the full redshift range and reproduces the galaxy bias from *Euclid*-internal simulations. I use the same approach for the *SKA2* sample, finding the same level of accuracy.

Specifically, I found the following values of the HOD parameters to best fit the specifications : for *Euclid* $M_{\min}^a = 11.03$, $M_{\min}^b = -0.185$, $M_{\min}^c = 0.575$, $M_{\min}^d = -0.107$; for *SKA2*, these were $M_{\min}^a = 10.24$, $M_{\min}^b = 2.53$, $M_{\min}^c = -0.610$, $M_{\min}^d = 0.064$, $M_{\text{ratio}} = 10$, $\sigma_{\log M} = 0.5$ and $\alpha_{\text{sat}} = 1$. This approach enables a halo modeling of the galaxy sample over the whole redshift range with 7 parameters : M_{\min}^a , M_{\min}^b , M_{\min}^c , M_{\min}^d , M_{ratio} , $\sigma_{\log M}$ and α_{sat} .

With this framework, all n -point polyspectra of galaxies can be computed through the halo model, and this involves integrals of the form:

$$I_{\mu}^{\beta}(k_1, \dots, k_{\mu}|z) = \int dM \frac{dn_h}{dM} \langle N_{\text{gal}}^{(\mu)} \rangle b_{\beta}(M, z) \times u(k_1|M, z) \cdots u(k_{\mu}|M, z) \quad (8)$$

with $\frac{dn_h}{dM}$ the halo mass function, $u(k|M, z)$ the halo profile, $b_{\beta}(M, z)$ the halo bias or order β , and $\langle N_{\text{gal}}^{(n)} \rangle \equiv \langle N_{\text{gal}}(N_{\text{gal}} - 1) \cdots (N_{\text{gal}} - (n - 1)) \rangle$ the number of n -uplets of galaxies (implicitly depending on halo mass).

For instance the number density of galaxies in a given redshift bin (in units galaxies/steradian) is given by

$$N_{\text{gal}}(i_z) = \int dV I_1^0(0|z) \quad (9)$$

where the integral runs implicitly over redshifts in the bin i_z , $dV = r^2(z) \frac{dz}{z}$ is the comoving volume per steradian and $r(z)$ is the comoving distance to redshift z

2.3. C_{ℓ}^{gal} and its covariance

Using the halo model, the power spectrum is standardly composed of 2-halo, 1-halo and shot-noise terms:

$$C_{\ell}^{2\text{h}}(i_z) = \int dV (I_1^1(k_{\ell}|z))^2 P(k_{\ell}|z) \Big| N_{\text{gal}}(i_z)^2 \quad (10)$$

$$C_{\ell}^{1\text{h}}(i_z) = \int dV I_2^1(k_{\ell}, k_{\ell}|z) \Big| N_{\text{gal}}(i_z)^2 \quad (11)$$

$$C_{\ell}^{\text{shot}}(i_z) = \int dV I_1^0(0|z) \Big| N_{\text{gal}}(i_z)^2 = 1/N_{\text{gal}}(i_z) \quad (12)$$

Fig. 1 shows the resulting power spectrum for the case of *SKA2* galaxies in the redshift bin $z = 0.46 - 0.53$, the median bin of the sample.

Two features are worth noting. First, the 1-halo term is roughly constant on multipoles $\ell \lesssim 2000$, but acquires a significant scale dependence afterwards. From Eq. 11 this scale dependence appears when we hit the radius of the typical host halo mass of the galaxy sample. Second, the high density of galaxies makes shot-noise subdominant, revealing the 1-halo term on a wide range of scales. Furthermore shot-noise can be subtracted exactly so what is important is its contribution to the covariance, where it contributes to the Gaussian part

$$C_{\ell, \ell'}^G = \frac{2 (C_{\ell}^{\text{clust}}(i_z) + C_{\ell}^{\text{shot}}(i_z))^2}{2\ell + 1} \delta_{\ell, \ell'} \delta_{i_z, j_z} \quad (13)$$

With this I find that all multipoles of the power spectrum of *SKA2* galaxies can be measured with $(S/N)_G > 5$ on the whole range $\ell \in [2, 20\,000]$ for all redshift bins. Even higher significance is reached for the *Euclid* photometric sample, which contains more

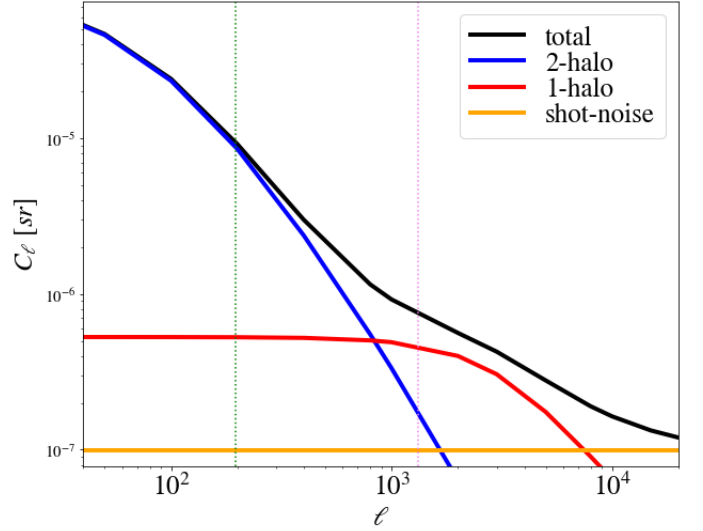


Fig. 1. Angular power spectrum of the *SKA2* galaxies in $z = 0.46 - 0.53$, and its different terms. Green dotted vertical line : limit of perturbation theory $k=0.15$ h/Mpc ; violet dotted vertical line : limit of the *Euclid* emulator $k=1$ h/Mpc.

galaxies. This shows that a huge statistical power will be present in the strongly non-linear regime, where the 1-halo dominates, both for *SKA2* and *Euclid*.

The Gaussian formula however does not capture the full covariance, especially on small scales. In this article I follow the equations for the non-Gaussian part of the covariance from Lacasa (2018), and the numerical approximation and implementation of Lacasa (2019). For the article to be self-contained, I summarize here the involved terms. The non-Gaussian covariance is composed of different contributions: super-sample covariance (SSC), braiding covariance, 1-halo term, 2-halo 1+3 term, 3-halo base-0 term and 4-halo third order term.

$$C_{\ell, \ell'}^{NG} = C_{\ell, \ell'}^{SSC} + C_{\ell, \ell'}^{\text{Braid}} + C_{\ell, \ell'}^{1\text{h}} + C_{\ell, \ell'}^{2\text{h}1+3} + C_{\ell, \ell'}^{3\text{h}base0} + C_{\ell, \ell'}^{4\text{h}3} \quad (14)$$

The super-sample covariance is given by

$$C_{\ell, \ell'}^{SSC} = \int dV_{ab} \Psi_{\ell}^{\text{sqz}}(z_a) \Psi_{\ell'}^{\text{sqz}}(z_b) \sigma^2(z_a, z_b) \Big| N_{\text{gal}}(i_z)^2 N_{\text{gal}}(j_z)^2$$

where $z_a \in i_z$, $z_b \in j_z$,

$$\sigma^2(z_a, z_b) = \frac{C_{\ell=0}^m(z_a, z_b)}{4\pi} = \frac{1}{2\pi^2} \int k^2 dk P(k|z_{ab}) j_0(kr_a) j_0(kr_b) \quad (15)$$

is the SSC kernel, and

$$\Psi_{\ell}^{\text{sqz}}(z) = 4 I_1^{\Sigma_2}(k_{\ell}|z) I_1^1(k_{\ell}|z) P(k_{\ell}|z) + I_2^1(k_{\ell}, k_{\ell}|z) \quad (16)$$

where

$$I_{\mu}^{\Sigma_2} = \frac{17}{21} I_{\mu}^1 + \frac{1}{2!} I_{\mu}^2 \quad (17)$$

is the sum of contributions from second order perturbation theory and second order bias

For Braiding covariance I use the Bij approximation from Lacasa (2019)

$$C_{\ell, \ell'}^{\text{Braid}} = 2 \Psi_{\ell, \ell'}^{\text{alt, int}}(i_z) \Psi_{\ell, \ell'}^{\text{alt, int}}(j_z) B_{\ell, \ell'}(i_z, j_z) \quad (18)$$

where

$$\Psi_{\ell,\ell'}^{\text{alt,int}}(i_z) = \int dV \Psi_{\ell,\ell'}^{\text{alt}}(z) \quad (19)$$

and

$$B_{\ell,\ell'}(i_z, j_z) = \sum_{\ell_a} \frac{2\ell_a + 1}{4\pi} \begin{pmatrix} \ell & \ell' & \ell_a \\ 0 & 0 & 0 \end{pmatrix}^2 C_{\ell_a}^{n_g^2}(i_z, j_z)$$

with

$$C_{\ell}^{n_g^2}(i_z, j_z) = \int dV_{ab} \bar{n}_{\text{gal}}(z_a)^2 \bar{n}_{\text{gal}}(z_b)^2 C_{\ell}^m(i_z, j_z) \left| \left(I_{\ell}^{n_g^2}(i_z) I_{\ell}^{n_g^2}(j_z) \right) \right| \quad (20)$$

and

$$I_{\ell}^{n_g^2}(i_z) = \int_{z \in i_z} dV \bar{n}_{\text{gal}}(z)^2. \quad (21)$$

Then come the 1-halo term

$$C_{\ell,\ell'}^{\text{1h}} = \frac{\delta_{i_z,j_z}}{4\pi} \int dV I_4^0(k_{\ell}, k_{\ell'}, k_{\ell'}|z) \left| N_{\text{gal}}(i_z) \right|^4, \quad (22)$$

the 2-halo 1+3 term

$$C_{\ell,\ell'}^{\text{2h1+3}} = \frac{2\delta_{i_z,j_z}}{4\pi} \int dV I_1^1(k_{\ell}|z) I_3^1(k_{\ell}, k_{\ell'}, k_{\ell'}|z) P(k_{\ell}|z) \left| N_{\text{gal}}(i_z) \right|^4 + (\ell \leftrightarrow \ell'), \quad (23)$$

the 3-halo base term

$$C_{\ell,\ell'}^{\text{3h-base0}} = \frac{\delta_{i_z,j_z}}{4\pi} \int dV 2 \left(I_1^1(k_{\ell}|z) P(k_{\ell}|z) \right)^2 I_2^{\Sigma_2}(k_{\ell'}, k_{\ell'}|z) \left| N_{\text{gal}}(i_z) \right|^4 + (\ell \leftrightarrow \ell') + \frac{4\delta_{i_z,j_z}}{4\pi} \int dV 2 I_1^1(k_{\ell}|z) I_1^1(k_{\ell'}|z) I_2^{\Sigma_2}(k_{\ell}, k_{\ell'}|z) \times P(k_{\ell}|z) P(k_{\ell'}|z) \left| N_{\text{gal}}(i_z) \right|^4, \quad (24)$$

and the 4-halo term from third order contributions

$$C_{\ell,\ell'}^{\text{4h-3}} = \frac{2\delta_{i_z,j_z}}{4\pi} \int dV 3! \left(I_1^1(k_{\ell}, z) \right)^2 I_1^1(k_{\ell'}, z) I_1^{\Sigma_3}(k_{\ell'}, z) \times P(k_{\ell}|z) P(k_{\ell'}|z) \left| N_{\text{gal}}(i_z) \right|^4 + (\ell \leftrightarrow \ell'). \quad (25)$$

where

$$I_{\mu}^{\Sigma_3} \equiv \frac{1023}{1701} I_{\mu}^1 + \frac{1}{3!} I_{\mu}^3 \quad (26)$$

is the sum of contributions from third order perturbation theory and third order bias.

Figure 2 shows all these terms in the case of the variance $C_{\ell,\ell}$ in the median bin of SKA2.

We see that the 3h-base and 4h-3 terms are negligible for this variance. In fact Lacasa (2019) already found that they have a negligible impact on the total covariance as well as parameter constraints up to $\ell_{\text{max}} = 2000$. Here I find this result to still hold to $\ell_{\text{max}} = 20000$.

Figure 2 however does not let us appreciate the complexity and importance of the other non-Gaussian terms, because it

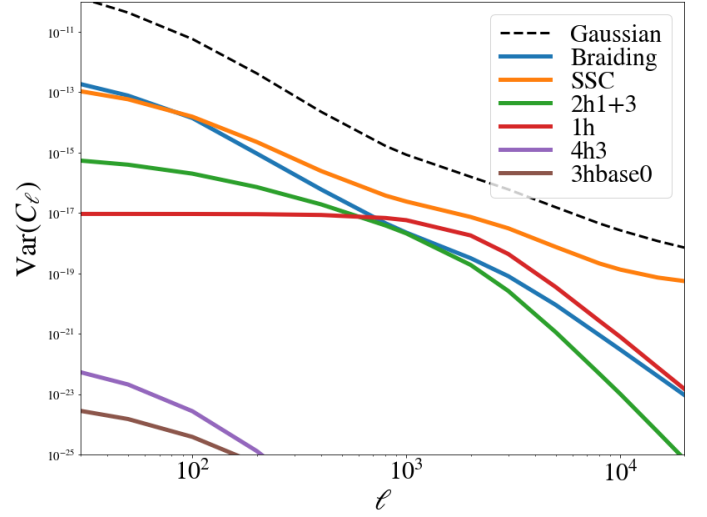


Fig. 2. Different contributions to the variance of C_{ℓ}^{gal} per individual multipole, for SKA2 galaxies in the median bin $z = 0.46 - 0.53$.

only focuses on the diagonal multipole by multipole. Also real analyses bin multipoles together, which can significantly change the amplitude of the terms ; for instance the Gaussian variance decreases strongly (typically as $1/\Delta\ell$). Thus all later results apply the binning of multipoles explained in Sect. 2.1. So, after binning, for the four most important non-Gaussian terms, Figure 3 shows the correlation matrix $C_{\ell,\ell'}/\sqrt{C_{\ell,\ell} \times C_{\ell',\ell'}}$, where each term is normalised by its own diagonal, to reveal its specific structure.

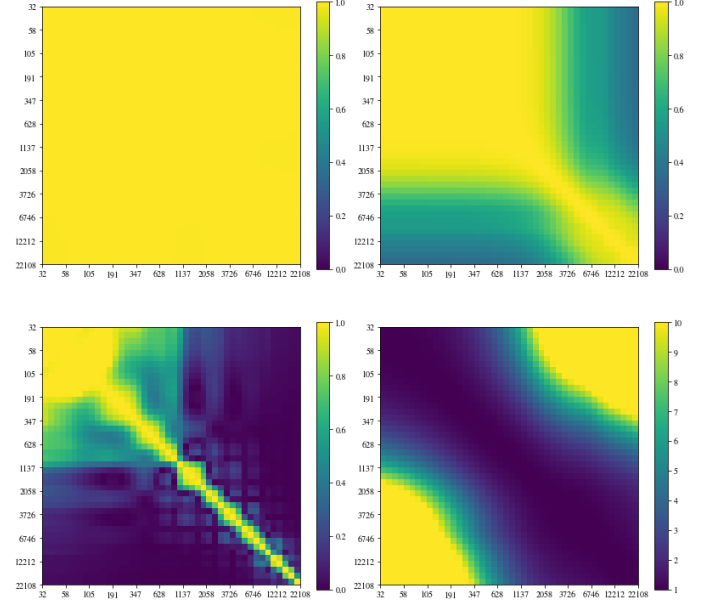


Fig. 3. Correlation matrices for the different non-Gaussian covariance terms, normalised by their own diagonal, for SKA2 galaxies in $z = 0.46 - 0.53$. From left to right and top to bottom: SSC, 1-halo, Braiding and 2-halo 1+3.

We see results consistent with Lacasa (2019) on large scales: SSC and 1-halo both yield 100% correlated covariance, Braiding is also strongly correlated albeit lower, and 2-halo 1+3 is minimal on the diagonal as it correlates large scales with small

scales. On top of this, a new behaviour appears at $\ell \gtrsim 2000$: the 1-halo stops being 100% correlated and gets closer to diagonal ; the same behaviour happens for Braiding covariance.

Now to see a first estimation of the relevance of these non-Gaussian terms, Fig. 4 shows the total covariance, including both the Gaussian and non-Gaussian contributions.

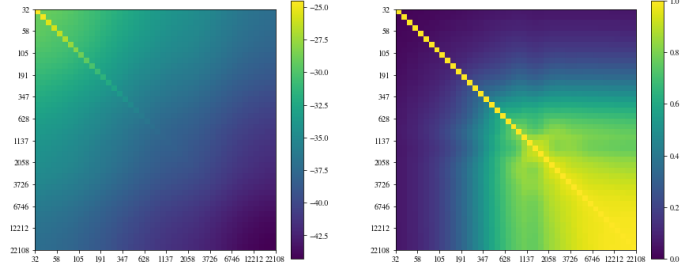


Fig. 4. Total covariance matrix, including both Gaussian and non-Gaussian terms, for SKA2 galaxies in $z = 0.46 - 0.53$. *Left:* covariance in log color scale. *Right:* correlation matrix.

Remembering that the Gaussian covariance only contributes on the diagonal, we see that the non-Gaussian term become relevant already at multipoles of a few hundreds, and at multipoles of a few thousands they dominate the matrix to the point that it becomes $>90\%$ correlated.

3. Fisher constraints

In this section, I use Fisher forecasts to quantify the information content in the galaxy angular power spectrum, and how it varies when extending the range of multipole of analysis. I use the covariance matrices shown in the previous section, rescaled with the f_{SKY} approximation

$$C_{\text{partial-sky}} = C_{\text{full-sky}} / f_{\text{SKY}} \quad (27)$$

to account for the partial sky coverage of the surveys. The Fisher information matrix in a given redshift bin then follows:

$$F_{\alpha\beta}(i_z) = \sum_{\ell, \ell' = \ell_{\min}}^{\ell_{\max}} \partial_{\alpha} C_{\ell}^{\text{gal}}(i_z) C_{\ell, \ell'}^{-1}(i_z, i_z) \partial_{\beta} C_{\ell'}^{\text{gal}}(i_z) \quad (28)$$

and the matrix summed over all bins is:

$$F_{\alpha\beta} = \sum_{i_z, j_z} \sum_{\ell, \ell' = \ell_{\min}}^{\ell_{\max}} \partial_{\alpha} C_{\ell}^{\text{gal}}(i_z) C_{\ell, \ell'}^{-1}(i_z, j_z) \partial_{\beta} C_{\ell'}^{\text{gal}}(j_z) \quad (29)$$

where α, β are model parameters, i.e. in the following both cosmological parameters ($\Omega_b h^2, \Omega_c h^2, H_0, n_s, \sigma_8, w_0$) and HOD parameters ($\alpha_{\text{sat}}, \sigma_{\log M}, M_{\text{ratio}}, M_{\text{min}}^a, M_{\text{min}}^b, M_{\text{min}}^c, M_{\text{min}}^d$). $\partial_{\alpha} C_{\ell}^{\text{gal}}$ is the derivative of the power spectrum with respect to the parameter α , and for simplicity I denote multipole bins with their center in all the following.

3.1. In angular scales

First, keeping ℓ_{\min} fixed, I study how the Fisher information varies when increasing the maximum multipole of analysis ℓ_{\max} . For this, I concentrate on the case of the three cosmological parameters that can best be constrained with full shape galaxy power spectra : σ_8, n_s and w_0 . In the case of the median redshift

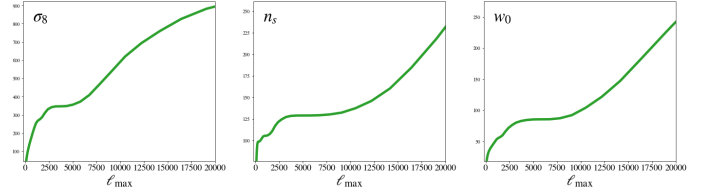


Fig. 5. Fisher information $F_{\alpha, \alpha}^{1/2}$ on σ_8, n_s and w_0 as a function of the angular cut ℓ_{\max} , for SKA2 galaxies in $z = 0.46 - 0.53$.

bin of SKA2, Figure 5 shows the information $F_{\alpha, \alpha}^{1/2}$ as a function of ℓ_{\max} . This quantity is indeed the inverse of the error bar on the parameter α before marginalisation on other model parameters.

We see a typical striking behaviour of the curves : when increasing ℓ_{\max} the information first rises steadily on linear and weakly non-linear scales, but this increase progressively slows down before coming to a stop around $\ell_{\max} \sim 2000$, a plateau is then present where information has saturated : adding these power spectrum measurements does not bring any (direct) information on cosmological parameters. The extension of this plateau depends on the considered parameter, but for all of them the plateau finally comes to an end and information rises again with a steep slope. The information brought after the plateau up to $\ell_{\max} = 20000$ is comparable to (for n_s) or larger than (for σ_8 and w_0) the information from linear/weakly non-linear scales before the plateau. This steep rise is the small scale miracle that gives its title to this article.

Now comes the question whether this qualitative behaviour is peculiar to this redshift bin and this survey. Concentrating on the case of Dark Energy, Figure 6 shows $F_{w_0, w_0}^{1/2}$ as a function of ℓ_{\max} for different redshift bins of SKA2, both raw (left) and after a rescaling to appreciate the qualitative behaviour of each curve (right). I selected 5 out of the 10 redshift bins to avoid overcrowding the plot, but the omitted bins follow the same qualitative behaviour as the one presented.

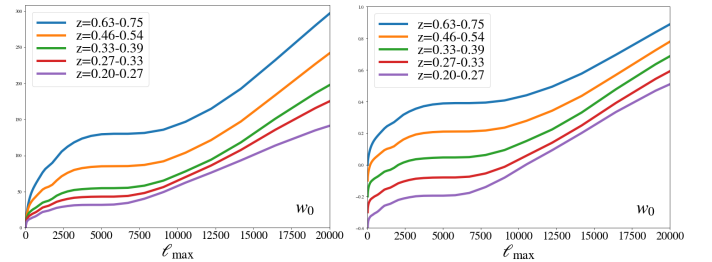


Fig. 6. *Left:* Fisher information on $w_0, F_{w_0, w_0}^{1/2}$, as a function of ℓ_{\max} for most redshift bins of SKA2, where the bins were selected to keep clarity of the plot. *Right:* same but all curves are rescaled to $[0,1]$ and an offset is added for readability.

We see that all curves follow the qualitative behaviour found previously, with a striking plateau where information saturates before rising again, the ‘‘small scale miracle’’. The location (and extent) of the plateau depends on redshift : it slowly moves to smaller angular scales at higher redshifts. I checked that this qualitative behaviour of the information content is also present for the *Euclid* survey, the main difference being that the plateau can move to even smaller scales as the sample goes to higher redshift (up to $\ell \sim 12000$ in the highest bin $z = 1.6 - 2.5$). I also checked whether this qualitative behaviour is also present for other model parameters, and found that it is also clearly present

for all the HOD parameters ; for the other cosmological parameters $\Omega_b h^2$ and $\Omega_c h^2$ (H_0 being basically unconstrained by the galaxy power spectrum) the picture is a bit less clear : a plateau can be seen in some redshift bins but not all, however the rise of information on small scales remains, which is the most important feature.

Before interpreting these results, we may wonder what these angular scales of the plateau correspond to in terms of physical scales, and whether the redshift evolution of the plateau could be explained by projection onto angles.

3.2. In physical scales

In this section, I want to define a cut-off of the power spectrum data vector in physical scales k_{\max} instead of angular scales ℓ_{\max} . This for two reasons : (i) it allows more natural and redshift-independent understanding of the considered scales and what they correspond to, and (ii) the range of validity of theoretical approaches to non-linearity (perturbation theory, halo model, emulators...) is usually stated in terms of physical scales.

A fixed cut-off in physical scales k_{\max} corresponds to a redshift-dependent cut-off in angular scales $\ell_{\max}(z) = k_{\max}/r(z)$ with the Limber approximation. That prescription works well for infinitesimal redshift bins and when all multipoles are available. However in the present case, there is the added complexity that I have predefined redshift and multipole bins. I chose to apply the prescription at the center of the redshift bin to obtain a first ℓ_{\max} , and then I cut at the multipole bin whose center is the closest to that ℓ_{\max} .

I defined 16 values of k_{\max} between 0.1 Mpc^{-1} –cut-off of the validity of perturbation theory– to 10 Mpc^{-1} –optimistic cut-off assuming future advances over the current emulators. In the lowest redshift bin, this can correspond to ℓ_{\max} above 20 000, hence why I defined multipole bins up to higher ℓ in Sect. 2.1.

Figure 7 shows the resulting information content $F_{\alpha,\alpha}^{1/2}$ as a function of k_{\max} for the cosmological parameters σ_8 , n_s and w_0 , in the case of the median redshift bin of SKA2.

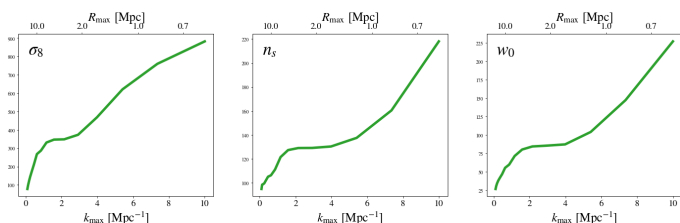


Fig. 7. Fisher information on σ_8 , n_s and w_0 as a function of the physical cut k_{\max} , for SKA2 galaxies in $z = 0.46 - 0.53$. The corresponding real-space cut $R_{\max} = 2\pi/k_{\max}$ is indicated in the upper x-axis.

We see that the typical behaviour found in Sect. 3.1, with a plateau of information and the “small scale miracle”, is still present. Furthermore, the plateau happens at a few Mpc^{-1} , which translates in real space to $\sim 2 \text{ Mpc}$. This is an interesting result as it basically corresponds to the limit of validity of current emulators for the matter power spectrum.

Then, concentrating on the case of Dark Energy, Figure 8 shows the information content on w_0 as a function of k_{\max} for different redshift bins of SKA2.

We see that the location (and extent) of the plateau is redshift dependent, moving to larger physical scales when increasing redshift. In fact, this explains why the angular shift of the plateau in Figure 6 was only weak : when increasing redshift, a

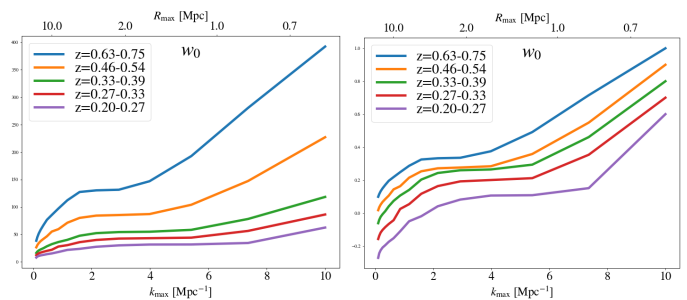


Fig. 8. Left: Fisher information on w_0 as a function of k_{\max} , for most redshift bins of SKA2. Right: same but all curves are rescaled to $[0,1]$ and an offset is added for readability. The curves are not always perfectly smooth because the translation of k_{\max} into ℓ_{\max} is approximate due to binning, as explained in the text.

fixed physical scale projects onto smaller angular scales, so both effects (physical mode and projection) go in opposite directions.

3.3. Interpretation

I now give a physical understanding for the presence and location of the plateau of information and the subsequent rise of information on highly non-linear scales.

First, we have seen that the plateau appears around $\ell \sim 2000$. Looking at Fig. 1, we see that this is a scale where the 1-halo term dominates the power spectrum and is still roughly constant. Looking at Fig. 2 we see that the non-Gaussian covariance is dominated by the SSC and 1-halo at this scale. And looking at Fig. 3 we see that these covariance terms are 100% correlated at this scale. So a first rough statistical picture is that on the scales of the plateau, we are measuring a (roughly) constant power spectrum whose error bars are 100% correlated. So adding scales does not refine the measurement of that constant, and hence the information content saturates.

From a more physical point of view, the 1-halo power spectrum corresponds on large scales to the shot-noise (sometimes called Poisson noise) of the halos. The large scale value of C_ℓ^{1h} is a weighted average of the halo number (divided by $N_{\text{gal}}(i_z)^2$), where massive halos have the more weight as they host more galaxies. So basically on large scales the 1-halo measures a single information : a weighted number of halos in the survey. At $\ell \sim 2000$ we have basically exhausted the constraining power of this information. Indeed there is a cosmic variance to the number of halos, which is given by the 1-halo trispectrum (which quantifies the variance due to the discreteness of halos / Poisson noise) and super-sample covariance (which quantifies the variance due to super-survey fluctuations which modulate the number of halos inside the survey). Once this constraining power has been exhausted, as long as C_ℓ^{1h} keeps (roughly) constant, adding scales does not bring anything new. Hence the information content saturates.

Second, we can now understand why this plateau ends and information rises again. The start of this rise depends on the cosmological parameter but is roughly around $\ell \sim 5000$. From Fig. 1, this is a scale where the C_ℓ^{1h} picks up a significant scale dependence. From Fig. 2 and 3, on these scales the SSC dominates the covariance and is still 100% correlated, while other sources of covariance become closer to diagonal. From a statistical point of view we are thus now able to extract information from the scale dependence of the power spectrum, and we are thus recovering constraining power. From a physical point

of view, on these smaller scales C_ℓ^{1h} stops being dominated by massive (and rare) halos and starts to probe the amount of less massive halos which are smaller ; we no more measure a single information and thus recover constraining power.

Finally, we can refine the picture to understand why the location and extent of the plateau depends on cosmological parameter and redshift.

First for cosmological parameters, the cosmological constraints in the highly non-linear regime come from the fact that by pushing to smaller scales we measure a weighted number of halos with different weights ; so basically we measure the halo mass function (which is sensitive to cosmology), with smaller scales allowing to probe smaller masses. The halo mass function is highly sensitive to σ_8 with a steep scaling at high mass, and the exponent of that scaling decreases significantly at lower masses which allows to quickly break degeneracies. This explains why the plateau of information for σ_8 ends the soonest in Fig. 5 : as soon as C_ℓ^{1h} stops being constant, its shape is violently sensitive to σ_8 due to the high scalings ; furthermore this scaling is completely different from that of the linear C_ℓ^{2h} which goes as σ_8^2 . By contrast, n_S shows a much longer plateau in Fig. 5 ; this is because what we need to constrain n_S is a high leverage arm in the scales k of the initial power spectrum. The halo mass function is more weakly sensitive to n_S (compared to σ_8), because what enters its prediction is $\sigma(R)$ the variance of the matter field smoothed at the halo radius scale, which is a convolution of $P(k)$ with a wide kernel. One needs to go to very small masses to probe small k in $P(k)$. This explains why in Fig. 5 the information on n_S starts to rise again only at smaller scales, and why the ratio of information after/before the plateau is more modest for n_S than σ_8 . For the Dark Energy equation of state, the situation is intermediate between σ_8 and n_S ; this is because the halo mass function is sensitive to w_0 , though not as much as σ_8 , and w_0 also has an influence on the comoving volume dV which enters C_ℓ^{1h} . Second for the redshift dependence, we see from Fig. 8 that the plateau extends to smaller scales at lower redshifts. This is basically due to sample selection : because the *Euclid* and *SKA* surveys are flux-limited (instead of volume-limited), at lower redshifts we have many more faint galaxies that live in light halos. So at low z C_ℓ^{1h} gets more contribution from less massive halos and will thus pick up a significant scale dependence only on smaller physical scales. This leads the plateau to extend to these smaller physical scales.

3.4. Marginalisation over astrophysics

One last issue we could worry about, is whether the cosmological information found on small scale is or not degenerate with the astrophysics. Figure 9 answers this question by showing the marginalised error bars on n_S and w_0 as a function of k_{\max} , for *SKA2* galaxies summed over all redshift bins.

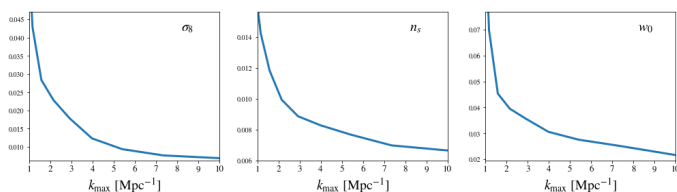


Fig. 9. Marginalised error bars on n_S and w_0 as a function of k_{\max} , for *SKA2* galaxies summed over all redshift bins..

We see that, despite marginalising over 7 HOD parameters there is a huge improvement of the cosmological errors when increasing k_{\max} . Quantitatively, when pushing from $k_{\max} = 1$ Mpc^{-1} to $k_{\max} = 10$ Mpc^{-1} , the error bar on σ_8 improves by a factor 8.8, the error bar on n_S improves by a factor 2.4, and the error bar w_0 improves by a factor 4.9. This is of high interest to study the current tension on σ_8 , constrain inflation and Dark Energy models.

4. Estimating the information in higher orders

Until now I have focussed the study on the information contained solely in the power spectrum. A first question that arises is whether the qualitative behaviours that I have found, with the plateau and the “small scale miracle”, can be expected for higher order statistics. Indeed, future surveys do plan to use this information, for instance at third order with the bispectrum.

From analytical arguments, I indeed expect a similar behaviour for higher order correlation functions / polyspectra. Indeed these polyspectra also get dominated by a 1-halo term in the highly non-linear regime. This 1-halo polyspectrum will also be constant on large scales and pick up a scale dependence at the radius corresponding to the typical host halo mass. So before that scale, the 1h information will be a constant equal to a weighted number of halo in the survey (with weights different from the power spectrum, preferring even more massive halos), and that constant will have a cosmic variance due to SSC and 1h covariance which will limit its constraining power.

A second question that arises is how much constraining power these higher orders can bring on top of the power spectrum. In other words, what is the fundamental limit to the constraining power of the galaxy density field, if we knew how to analyse it optimally ?

If the galaxy density field were Gaussian, the power spectrum would be the optimal statistic, so the limit would be given by the Fisher information in the power spectrum with a Gaussian covariance. The non-linearity however introduces another fundamental limit : super-sample covariance. Indeed, SSC comes from super-survey modes which change the matter density in the survey by an amount δ_b called the background shift. [Wagner et al. \(2015\)](#) has shown that a portion of Universe with this background shift evolves identically to a portion of Universe with a different cosmology. This is the basis of the so-called separate universe approach. Observationally, this means that all cosmological observables, and in particular all statistics of the galaxy density field, will behave as in this different cosmology. Super-sample covariance thus sets a fundamental limit to the cosmological constraints achievable from a given survey volume, independently of the statistics used. Figure 10 hence compares the Fisher information with the Gaussian+SSC covariance on one hand and the total power spectrum covariance on the other hand, in the case of constraints on σ_8 , n_S and w_0 summed over all redshift bins of *SKA2*.

We see that there is indeed significant information that can be gained beyond the power spectrum, and that this gain rises rapidly when pushing to smaller scales. To be more quantitative, Table 1 gives the increase of information on σ_8 , n_S and w_0 for some scale cuts.

The gain is the most spectacular for σ_8 , more modest but still interesting for n_S , and important for w_0 . This can be understood because σ_8 highly influences the amount of non-linearity and thus high order statistics allow excellent constraints by breaking degeneracies ; for instance on perturbative scales the power spectrum scales as $(b\sigma_8)^2$ while the bispectrum scales as $b^3\sigma_8^4$, where

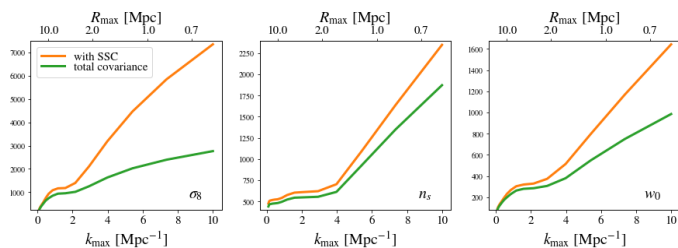


Fig. 10. Fisher information on σ_8 , n_S and w_0 as a function of the physical cut k_{\max} , for SKA2 galaxies summed over all redshift bins. The green lower curve shows the power spectrum information with the total covariance, while the orange upper curve uses only the Gaussian + super-sample covariance, as an estimate of the fundamental limit of the information in the galaxy density field.

	1 Mpc ⁻¹	2 Mpc ⁻¹	5 Mpc ⁻¹	10 Mpc ⁻¹
σ_8	+26%	+32%	+114%	+166%
n_S	+9.5%	+11%	+17%	+25%
w	+16%	+15%	+43%	+67%

Table 1. Improvement of the Fisher information on σ_8 , n_S and w_0 between the Gaussian+SSC and the total covariance, depending on the scale cut in the analysis, using all redshift bins of SKA2.

b is the galaxy bias. For n_S , as argued in Sect. 3.3 constraints in the highly non-linear regime come from probing small mass halos; however high order statistics preferentially probe extreme events i.e. massive halos, so the improvement they bring is more modest. Finally for w_0 the situation is intermediate between n_S and σ_8 because it impacts the mass function at all masses, and because it also gets constrained by the comoving volume dV whose constraints are improved by high orders. Indeed, for the numerator of the power spectrum (i.e. without the $1/N_{\text{gal}}(i_z)^2$ normalisation), the 2-halo term scales as dV^2 while the 1-halo scales as dV ; correspondingly the bispectrum has terms in dV^3 , dV^2 and dV , thus high order statistics allow to better constrain the comoving volume by breaking degeneracies.

5. Discussion

I have thus shown that the galaxy angular power spectrum can contain valuable cosmological information in the highly non-linear regime dominated by the 1-halo term. In this regime the information rises steeply with a slope comparable to that in the linear regime, which can yield huge improvement to constraint on the Dark Energy equation of state.

To realise these promises relies on reaching the “small scale miracle” which lies on scales $k > 3 \text{ Mpc}^{-1}$. This is currently out of reach of the best methods to predict the matter power spectrum such as the *Euclid* emulator Knabenhans et al. (2019), at least at the 1% precision level. One can however hope to reach these scales in future as the needed improvement of reach is a factor < 10 ; there is for instance a proposal that could reach these scales by (Hannestad & Wong 2019).

I note that predicting matter statistics is not a sufficient condition to realise the small scale miracle. To my knowledge, only galaxy and intensity mapping can reach this regime, as for instance cosmic shear gets dominated by shape noise earlier on. So we further need a modeling of galaxies to these scales, which brings the challenge of galaxy formation physics. To my eyes the most promising prediction framework for this is the halo model.

There are issues often raised against the halo model but recent progresses could solve them. For instance the problem with mass conservation and large scales is solved in the Extended Halo Model (EHM) of Schmidt (2016); the problem of imprecision in the transition regime between 2-halo and 1-halo can be solved by the Amended Halo Model (AHM) of Chen & Afshordi (2019). Furthermore, none of these issues affect the small scale miracle, which lies in the highly non-linear regime where the 1-halo term is dominant.

Using the 1-halo term for cosmological constraints is not usual in traditional galaxy surveys. However this has been done routinely in other domains. For example in the case of analyses of the thermal Sunyaev-Zel’dovich (tSZ) effect, the angular power spectrum is entirely dominated by the 1-halo term on all scales that have been observed to date. And cosmological constraints have been extracted out of the tSZ power spectrum for instance by Planck Collaboration et al. (2014, 2016). It has been shown that there is a high interest in analysing higher order statistics: for instance in Planck Collaboration et al. (2014) the tSZ bispectrum gave cosmological constraints of comparable power to those of the power spectrum, both analyses being in fact limited by uncertainties in the astrophysics of the cluster gas. Furthermore, Hurier & Lacasa (2017) showed that the tSZ bispectrum, power spectrum and cluster counts have a great synergy that breaks degeneracies between cosmological and astrophysical parameters. In the case of the galaxy power spectrum, Lacasa (2019) showed that the inclusion of non-Gaussian covariance terms in the covariance decreases the degeneracies between cosmological and HOD parameters, and Lacasa & Rosenfeld (2016) showed that the inclusion of cluster counts allows to break some of these degeneracies.

I conclude that there is high interest in pushing the analyses of galaxy clustering to scales of a few Mpc^{-1} to 10 Mpc^{-1} , dominated by the 1-halo term. This regime will be measured “for free” with future high resolution surveys of the large scale structure, and it does contain cosmological information which can be disentangled from the astrophysical modeling. Reaching these scales will allow much better understanding of Dark Energy, decreasing error bars by a factor of a few compared to the perturbative regime. High order statistics and probe combination with clusters will bring even more improvement and break some of the remaining degeneracies with astrophysics.

Acknowledgements

Part of this work was supported by funds of the Département de Physique Théorique, Université de Genève. Part of this work was supported by a postdoctoral grant from Centre National d’Études Spatiales (CNES). Some of the computations made use of the CLASS code (Blas et al. 2011).

References

- Abell, P. A. et al. 2009 [arXiv:0912.0201]
- Balmès, I., Rasera, Y., Corasaniti, P.-S., & Alimi, J.-M. 2014, MNRAS, 437, 2328
- Blas, D., Lesgourgues, J., & Tram, T. 2011, J. Cosmology Astropart. Phys., 2011, 034
- Bull, P. 2016, ApJ, 817, 26
- Cataneo, M., Emberson, J. D., Inman, D., Harnois-Deraps, J., & Heymans, C. 2019a, arXiv e-prints, arXiv:1909.02561
- Cataneo, M., Lombriser, L., Heymans, C., et al. 2019b, MNRAS, 488, 2121
- Chen, A. Y. & Afshordi, N. 2019, arXiv e-prints, arXiv:1912.04872
- Contigiani, O., Vardanyan, V., & Silvestri, A. 2019, Phys. Rev. D, 99, 064030
- Cooray, A. & Sheth, R. 2002, Phys. Rep., 372, 1

- Euclid Collaboration, Blanchard, A., Camera, S., et al. 2019, arXiv e-prints, arXiv:1910.09273
- Giblin, B., Cataneo, M., Moews, B., & Heymans, C. 2019, arXiv e-prints, arXiv:1906.02742
- Hannestad, S. & Wong, Y. Y. Y. 2019, arXiv e-prints, arXiv:1907.01125
- Hoffmann, K., Bel, J., Gaztañaga, E., et al. 2015, MNRAS, 447, 1724
- Hurier, G. & Lacasa, F. 2017, A&A, 604, A71
- Knabenhans, M., Stadel, J., Marelli, S., et al. 2019, MNRAS, 484, 5509
- Kobayashi, Y., Nishimichi, T., Takada, M., & Takahashi, R. 2019, arXiv e-prints, arXiv:1907.08515
- Lacasa, F. 2018, A&A, 615, A1
- Lacasa, F. 2019, arXiv e-prints, arXiv:1909.00791
- Lacasa, F. & Rosenfeld, R. 2016, J. Cosmology Astropart. Phys., 8, 005
- Lange, J. U., van den Bosch, F. C., Zentner, A. R., et al. 2019, arXiv e-prints, arXiv:1909.03107
- Laureijs, R. et al. 2011 [arXiv:1110.3193]
- Lopes, R. C. C., Voivodic, R., Abramo, L. R., & Sodr , Jr., L. 2018, J. Cosmology Astropart. Phys., 9, 010
- Lopes, R. C. C., Voivodic, R., Abramo, L. R., & Sodr , Jr., L. 2019, J. Cosmology Astropart. Phys., 7, 026
- Loureiro, A., Moraes, B., Abdalla, F. B., et al. 2019, MNRAS, 485, 326
- Maartens, R., Abdalla, F. B., Jarvis, M., & Santos, M. G. 2015, PoS, AASKA14, 016
- Ntampaka, M., Eisenstein, D. J., Yuan, S., & Garrison, L. H. 2019, arXiv e-prints, arXiv:1909.10527
- Planck Collaboration, Ade, P. A. R., Aghanim, N., et al. 2014, A&A, 571, A21
- Planck Collaboration, Aghanim, N., Akrami, Y., et al. 2018, ArXiv e-prints [arXiv:1807.06209]
- Planck Collaboration, Aghanim, N., Arnaud, M., et al. 2016, A&A, 594, A22
- Ryu, S. & Lee, J. 2019, arXiv e-prints, arXiv:1910.07690
- Schmidt, F. 2016, Phys. Rev. D, 93, 063512
- Tansella, V. 2018, Phys. Rev. D, 97, 103520
- Tinker, J., Kravtsov, A. V., Klypin, A., et al. 2008, ApJ, 688, 709
- Tinker, J. L., Robertson, B. E., Kravtsov, A. V., et al. 2010, ApJ, 724, 878
- Tr ster, T., S nchez, A. G., Asgari, M., et al. 2019, arXiv e-prints, arXiv:1909.11006
- Wagner, C., Schmidt, F., Chiang, C.-T., & Komatsu, E. 2015, MNRAS, 448, L11
- Zehavi, I., Zheng, Z., Weinberg, D. H., et al. 2011, ApJ, 736, 59